Applied Catalysis A: General 405 (2011) 142–148

Contents lists available at ScienceDirect

Applied Catalysis A: General

journal homepage: www.elsevier.com/locate/apcata

Mesostructured Ni-doped ceria as an efficient catalyst for styrene synthesis by oxidative dehydrogenation of ethylbenzene

Jie Xu [a], Bing Xue [a], Yong-Mei Liu [b], Yong-Xin Li [a,*], Yong Cao [b,**], Kang-Nian Fan [b]

[a] College of Chemistry and Chemical Engineering, Changzhou University, Gehu Road 1, Changzhou, Jiangsu 213164, PR China
[b] Shanghai Key Laboratory of Molecular Catalysis and Innovative Materials, Department of Chemistry, Fudan University, Shanghai 200433, PR China

ARTICLE INFO

Article history:
Received 15 March 2011
Received in revised form 27 May 2011
Accepted 2 August 2011
Available online 10 August 2011

Keywords:
Ceria
Nickel
Oxidative dehydrogenation (ODH)
Ethylbenzene
Styrene

ABSTRACT

Mesostructured doped $Ce_{1-x}M_xO$ catalysts (M = Al, Sn, Zr, Mn, and Ni) with large surface area prepared *via* template-assisted precipitation method have been tested for the oxidative dehydrogenation (ODH) of ethylbenzene (EB) to styrene. Several techniques including N_2 desorption–adsorption, X-ray diffraction, H_2-temperature programmed reduction (H_2-TPR), total oxygen storage capacity (OSC), and X-ray photoelectron spectroscopy (XPS) were applied to characterize the physicochemical properties of the as-synthesized materials. Of the $Ce_{1-x}M_xO$ catalysts tested, the CeNiO composite containing 10 mol% Ni demonstrates the highest ST yield of 55% with long-term stability for ODH of EB under 450 °C. By analysis of H_2-TPR and total OSC characterization profiles, the superior performance of $Ce_{0.90}Ni_{0.10}O$ catalyst can be attributed to the dramatic improvement in oxygen mobility and storage capacity of the ceria materials, resulting from the introduction of Ni species into ceria cubic structure and hence a further shrinkage of ceria lattice. A catalytic mechanism *via* a simple surface redox cycle has been tentatively proposed based on the XPS results.

© 2011 Elsevier B.V. All rights reserved.

1. Introduction

Styrene (ST) is one of the most important chemicals in the petrochemical industry for the production of polystyrene, acrylonitrile–butadiene–styrene (ABS) terpolymer, styrene–butadiene rubber (SBR), and so forth [1–3]. In 2009, the worldwide production of ST was more than 23 megatons [4]. Commercially, ST is mainly produced by direct dehydrogenation of ethylbenzene (EB), over K_2O-promoted Fe_2O_3 catalysts in the presence of a large quantity of steam at high temperature (600–650 °C) [5,6]. Due to its highly endothermic nature, this conventional process suffers from some disadvantages such as the thermodynamic limitation, irreversible catalyst deactivation and coke deposition [1,7]. Alternatively, the oxidative dehydrogenation (ODH) process of EB to ST in the presence of O_2 has attracted considerable attention since it can be operated under lower temperatures and the EB conversion would not be equilibrium limited [8–10].

A variety of catalytic systems, including amorphous $AlPO_4$ [1], CaO/SiO_2 [11], MnO_2/SiO_2 [12], $Mg(VO_4)_2$–MgO [13], and $V_2O_5/CeO_2/Al_2O_3$ [14], have been investigated for the process of the ODH of EB recently. To date, the most promising catalysts suggested for the process have been confined to several nanostructured carbon materials including onion like carbon (OLC) [9,15] or carbon nanofibers (CNF) [16,17], which have exhibited high conversion (>60%) of EB as well as high selectivity (>80%) to ST at 450–500 °C. Nevertheless, due to their properties of fine powder [16–18] and intrinsically low resistance to combustion of the materials in oxidative gas, the carbon-based catalysts cannot be extensively employed in the industrial application. In this context, it is highly desired to develop a newly robust catalyst applicable for the ODH of EB.

Ceria is one of the key components in the catalyst formulations for many industrially important reactions, e.g. three-way-catalysts (TWC) for automobile exhaust treatment [19,20], CO oxidation [21], and low temperature water-gas shift reaction [22,23]. The success of ceria in various applications is largely attributed to its unique combination of an elevated oxygen transport capacity with the ability to shift easily between Ce^{3+} and Ce^{4+} states, i.e. oxygen storage/release capacities (OSC) [14,24]. Despite this, the use of pure CeO_2 is highly discouraged because of its poor thermostability at high temperatures, thereby losing its crucial OSC characteristics [25]. To overcome the drawback, other transition metal ions are normally introduced into the ceria cubic structure, resulting in the formation of a defective fluorite-structured solid solution. Such modifications may confer new properties to the materials such as better resistance to sintering and higher OSC for various reactions, thus leading to totally different catalytic behavior [26].

* Corresponding author. Tel.: +86 519 86330135.
** Corresponding author. Tel.: +86 21 55665287.
E-mail addresses: liyxluck@126.com (Y.-X. Li), yongcao@fudan.edu.cn (Y. Cao).

0926-860X/$ – see front matter © 2011 Elsevier B.V. All rights reserved.
doi:10.1016/j.apcata.2011.08.001

More recently, we have reported that mesostructured ceria materials with high accessible specific areas can catalyze the ODH of EB at *ca.* 450 °C [27]. Whereas, the catalytic performance in terms of ST productivity achieved over the mesostructured ceria catalysts was still lower (22.7% convention of EB with 87.3% selectivity to ST) for the further application. In view of the aforementioned modifications for ceria materials, we envisioned that it would be of interest to explore the doped ceria materials for the ODH of EB. Herein, we report the development of a mesostructured Ni-doped ceria catalyst with enhanced activity and stability for the ODH of EB. Our results have revealed that the prominent increase of oxygen capacity combined with storage capacity, after the introduction of Ni species with an optimal amount, is indispensable for an efficient ceria-based catalyst.

2. Experimental

2.1. Catalyst preparation

$Ce_{1-x}M_xO$ (M = Al, Sn, Zr, Mn, and Ni, *x* denoted the molar ratio of M of to Ce) materials with high surface areas were synthesized *via* a previously established template-assisted precipitation method [28,29]. Typically, 4.5 mmol of $Ce(NO_3)_3$, the corresponding nitrate hydrate precursors (0.5 mmol), and CTAB (1.09 g) were dissolved in 100 ml of distilled water. Then, 150 ml of NaOH solution (0.16 mol L^{-1}) was added into the solution under stirring. The mixture was then maintained in a sealed glass vessel under stirring for 3 days. After aging at 90 °C for 3 h, the as-obtained precipitate was filtered and washed with hot water (~80 °C) for several times to remove the residual CTAB. The resultant powder was dried at 100 °C for 6 h and then calcined at 500 °C for 4 h. For the sake of comparison in the following catalytic, the oxalate gel co-precipitation method [30] was also employed to synthesize the Ni-doped ceria sample (designated as $Ce_{1-x}Ni_xO$–CP).

2.2. Characterization

Nitrogen sorption at −196 °C was measured using a Micromeritics TriStar 3000 after the samples were degassed (1.33×10^{-2} Pa) at 300 °C overnight. The specific surface area was calculated using the Brunauer–Emmet–Teller (BET) method, and pore size distribution was determined by the Barret–Joyner–Halenda (BJH) method.

TEM analysis was carried out with a JEOL 2010 electron microscope operating at 200 kV. Before being transferred into the TEM chamber, the samples dispersed in ethanol were deposited onto a carbon-coated copper grid and then quickly moved into the vacuum evaporator.

Structural analysis of CeO_2 and the doped ceria samples was carried out on a Bruker D8 Advance X-ray diffractometer equipped with a graphite monochromator, operating at 40 kV and 40 mA and employing nickel-filtered Cu-Kα radiation (λ = 1.5418 Å).

Temperature programmed reduction (TPR) profiles were obtained on a homemade apparatus. 100 mg of the samples were pretreated in a mixed gas (O_2/N_2 = 1/8) at 450 °C for 30 min and cooled to room temperature. Subsequently, the samples were reduced with 5% H_2/Ar at 40 mL min^{-1} with a ramping rate of 5 °C min^{-1} to 910 °C. The H_2 consumption was monitored by a TCD detector.

Thermal gravimetric analysis (TGA), as well as temperature-programmed oxidation (TPO) measurements of the fresh and spent catalysts, was conducted on a Perkin–Elmer TGA 7 analyzer. The sample was placed in an α-Al_2O_3 cumber and heated in flowing air (50 mL min^{-1}) from room temperature to 800 °C at a rate of 20 °C min^{-1}.

X-ray photoelectron spectra (XPS) analysis was performed on a Perkin–Elmer PHI 5000C spectrometer using Mg Kα radiation (1253.6 eV, pass energy of 20.0 eV). The carbonaceous C 1*s* line (284.6 eV) was used as the reference to calibrate the binding energies (BE).

2.3. Measurements of catalytic activity

The activity of the catalysts for the ODH of EB was measured in the temperature range of 350–500 °C at atmospheric pressure using a fix-bed, down-flow, tubular quartz reactor (i.d. 4 mm, length 400 mm). Approximately 50 mg of catalyst, in the form of 60–80 mesh particles, was used and mixed with 300 mg of SiC grains of similar size for best temperature control for each run. EB was evaporated at 35 °C in flowing N_2 and subsequently mixed with O_2. The corresponding flow rate of EB, O_2, and N_2 is fixed at 0.5, 0.4 and 20 mL min^{-1}, respectively. Prior to testing, the catalysts were pretreated in a mixed gas (O_2/N_2 = 1/8) at 450 °C for 30 min. The products were analyzed by an on-line gas chromatography (Agilent GC 6820 equipped with FFAP column for hydrocarbons and TDX-01 column for permanent gas analysis, coupled with FID and TCD detectors, respectively). The carbon balance was maintained closed to 100 ± 5% and the CO_x content was additionally monitored after catalytic combustion of organic species in a final total oxidation reactor. The data of catalytic performance was acquired after 2 h from the start of the reaction to obtain the steady result.

2.4. Total OSC measurement

The measurement of total OSC was tested at 450 °C. 25 mg of catalyst (60–80 mesh) was placed in a quartz U-shaped reactor. The concentrations of the three components (H_2, H_2O, and He) in the outlet gas were monitored by an on-line mass spectrometer (Balzers OmniStar). A sample was exposed to alternating H_2 (40 mL min^{-1} for 10 s) and He (40 mL min^{-1} for 80 s) pulses, and the alternating pulsation lasted until the signal intensity of H_2 reached a balance. Total OSC was calculated by integrating the H_2 consumed (mmol [O] g^{-1}).

3. Results and discussions

3.1. Catalyst tests

The catalytic performance of CeO_2 and a series of doped ceria samples in the ODH of EB was tested with the O_2/EB ratio of n_{O2}/n_{EB} = 0.8 at 450 °C. In all cases, the major product in the reaction is ST, accompanied with a small amount of oxygenates (e.g. benzaldehyde or benzyl alcohol) and/or carbon oxides. As shown in Fig. 1, the pure CeO_2 gives a relatively low EB conversion (26.4%). After doping of Al and Zr (10 wt%), the ceria catalysts demonstrated a poorer catalytic activity with a falling by *ca.* 10% of EB conversion. In sharp contrast, the dopants of Sn, Mn, and Ni with the same amount exhibit an apparent improvement of catalytic activity. The maximum catalytic performance is obtained over the $Ce_{0.90}Ni_{0.10}O$ sample with an excellent EB conversion of 63.8%, allowing a highest yield of ST. In summary, the order of the steady activity of doped ceria at 450 °C is as follows: $Ce_{0.90}Ni_{0.10}O > Ce_{e0.90}Mn_{0.10}O > Ce_{0.90}Sn_{0.10}O > CeO_2 > Ce_{0.90}Zr_{0.10}O > Ce_{0.90}Al_{0.10}O$.

To evaluate the effects of the dopant amount on the catalytic behavior, the catalytic performance of a series of $Ce_{1-x}Ni_xO$ samples are summarized in Table 1. It is remarkable that a little amount of Ni doping (5%) into the ceria could drastically elevate the catalytic activity, with a twofold increase of EB conversion. However, higher amount of Ni with 20% would compromise the catalytic activity.

Table 1
Catalytic performances of CeO_2 and Ni-doped ceria catalyst.

Catalyst	Con. of EB (%)	Sel.%			Yield of ST (%)
		ST	CO_x	Others[a]	
CeO_2	26.4	85.4	6.3	8.3	22.5
$Ce_{0.95}Ni_{0.05}O$	43.6	85.1	2.9	12.0	37.1
$Ce_{0.90}Ni_{0.10}O$	63.8	86.3	3.4	10.3	55.1
$Ce_{0.80}Ni_{0.20}O$	50.6	87.7	2.9	9.4	44.4
$Ce_{0.90}Ni_{0.10}O$-CP	40.8	86.4	3.7	9.9	35.3

[a] Benzaldehyde or/and benzyl alcohol.

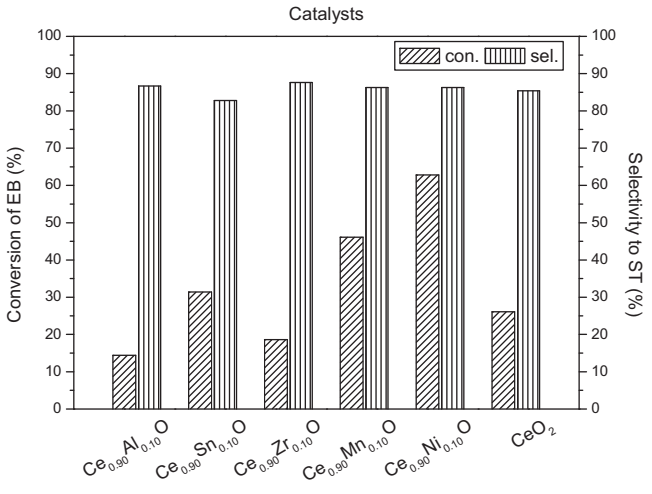

Fig. 1. Catalytic performances of pure CeO_2 and various metal-doped ceria catalysts.

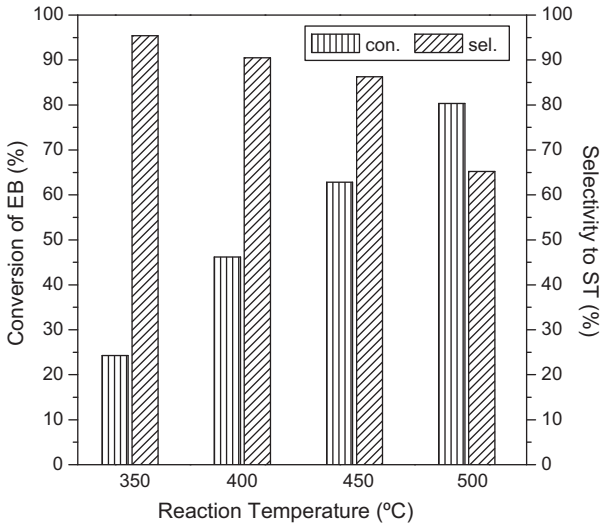

Fig. 2. Effect of reaction temperature on the activity and selectivity of the $Ce_{0.90}Ni_{0.10}O$ sample in ODH of EB.

One can see that when the amount of Ni is up to 10%, the EB conversion reaches the maximum, affording a substantially high ST yield of 55.1%. Additionally, the $Ce_{0.90}Ni_{0.10}O$-CP sample prepared by the co-precipitation method was employed in the ODH of EB at the same reaction condition. As indicated in Table 1, the $Ce_{0.90}Ni_{0.10}O$-CP catalyst gives an inferior catalytic activity, in contrast to the $Ce_{0.90}Ni_{0.10}O$ sample with identical amount of Ni.

The catalytic activity of the Ni-doped ceria catalysts is also found to be strongly dependent on the reaction temperature. To determine the possible low-temperature performance of the Ni-doped ceria catalysts, the catalytic performance of the $Ce_{0.90}Ni_{0.10}O$ catalyst at temperatures between 350 and 500 °C was investigated. Fig. 2 plots the ODH of EB over the $Ce_{0.90}Ni_{0.10}O$ catalyst as a function of reaction temperature. It is found that the $Ce_{0.90}Ni_{0.10}O$ catalyst displays a poor catalytic activity at 350 °C. As the reaction temperature increases, the EB conversion increases rapidly with a smooth decrease of the ST selectivity from 95.4% to 65.2%. The decrease of the selectivity to the target product can be ascribed to the consecutive oxidation of ST or direct oxidation of EB into oxygenates and/or CO_x at the elevated temperature [1]. Concerning a higher ST yield, the temperature of 450 °C is the ratio of choice.

Besides the activity and selectivity, stability of the catalyst is also of paramount importance in ODH of EB to ST. Herein, Ni-doped ceria catalysts, together with the pure CeO_2, were tested in the ODH of EB at 450 °C for 12 h. The evolution of the catalytic performance as a function of reaction time for the catalysts is compiled in Fig. 3. The ST selectivity for all samples remains constant at a value of *ca.* 85%, with the $Ce_{0.80}Ni_{0.20}O$ sample being appreciably higher selective (87.2%) than its counterparts (not shown here). It is worthy to note that, in our previous report [27], the pure mesostructured ceria catalyst underwent an apparent decrease of EB conversion during the initial 2 h, which was due to the decrease of the BET surface. In contrast, after the reaction for 12 h, the BET surface area and pore volume of the spent Ni-doped ceria catalyst have not represented any apparent changes (±10%). Therefore, it could be concluded that the doping of Ni species facilitates the maintenance of the mesostructure of the ceria sample.

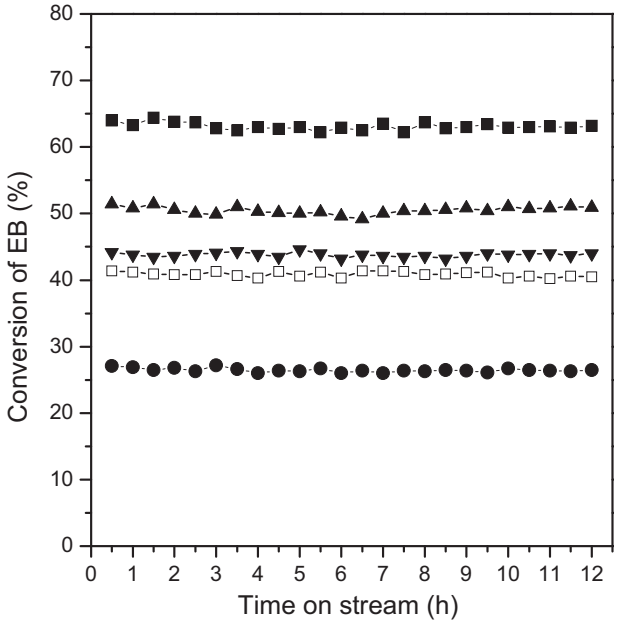

Fig. 3. EB conversion and selectivity to ST as a function time on stream obtained on CeO_2 and Ni-doped ceria catalysts at 450 °C (■: $Ce_{0.90}Ni_{0.10}O$, ▲: $Ce_{0.80}Ni_{0.20}O$, ▼: $Ce_{0.95}Ni_{0.05}O$, ●: CeO_2, □: $Ce_{0.90}Ni_{0.10}O$-CP).

Table 2
Comparison of the catalytic performances of different catalyst systems for ODH of EB.

Catalyst	O_2/EB ratio	SV ($mL\ g_{catal.}^{-1}\ min^{-1}$)	T (°C)	Con. of EB (%)	Sel. to ST (%)	Yield of ST (%)	STY ($mmol_{ST}\ g_{catal.}^{-1}\ h^{-1}$)	Ref.
$Ce_{0.90}Ni_{0.10}O$	0.8	418	450	64	86	55	14.8	This work
$Ce_{0.90}Ni_{0.10}O$	0.8	250	450	70	75	52	14.0	This work
20%V-Mg-O	2	300	530	32	96	31	11.0	[13]
6%V/CeZr/SiO_2	3	30	400	20	92	18	2.0	[6]
$FePO_4$-A-450	2	61	440	24	86	21	0.16	[2]
$AlPO_4$	2	61	440	44	99	44	0.35	[2]
Nanotube-2	0.5	1	400	29	94	27	3.4	[37]
CNF	1	50	400	56	85	48	1.27	[8]
OLC	1	250	510	92	68	63	8.38	[9]

Table 2 compares the catalytic performance of $Ce_{0.90}Ni_{0.10}O$ in the ODH of EB with that of other reported catalysts. It should be stressed that the experimental conditions in the literature concerning the reaction may deviate from each other. Nevertheless, a rough comparison is still feasible in the present study. As summarized in Table 2, the $Ce_{0.90}Ni_{0.10}O$ catalyst gives a high catalytic performance even under high space velocity condition. At 450 °C and total space velocity of 415 $mL\ g_{catal.}^{-1}\ min^{-1}$, the obtained space–time yield (STY) for ST production is 14.8 $mmol_{ST}\ g_{catal.}^{-1}\ h^{-1}$ while the selectivity to ST is 86%. These values compare favorably with the results reported on most conventional metal oxide catalysts, wherein the space velocities are much lower and the EB conversions are around 35%. Of particular note is that such ODH performance is appreciably higher than those of the carbon-based catalytic systems reported in the literature. At this juncture, the above catalytic evaluation strongly manifests that the present mesostructured $Ce_{0.90}Ni_{0.10}O$ material can serve as a promising catalyst for styrene synthesis from the ODH of EB.

3.2. Structure characterization

The textural properties of the ceria-based samples were studied by the N_2 adsorption–desorption methods. The values of specific surface area, mean pore diameter and pore volume are summarized in Table 3. Pure CeO_2 prepared *via* template-assisted precipitation method possesses a specific surface area of 175 $m^2\ g^{-1}$. After the incorporation of the second metal anion into the ceria, a marked decrease of the surface area and pore volume with increase of Ni amount is observed. Fig. 4 depicts the pore diameter distribution and the corresponding N_2 adsorption–desorption isotherms of the pure CeO_2 sample. The isotherm is of type IV with a hysteresis loop ranging from 0.6 to 0.9 p/p_0, a typical of the mesostructured material. Furthermore, the pore size distribution calculated from the desorption branch of CeO_2 shows that the pore diameter ranges from 4 nm to 30 nm with a maximum at around 9.6 nm (the inset to Fig. 4). By contrast, the doped ceria sample containing with 10 wt% Ni represents a quite narrow size distribution centered at 3.7 nm. These results suggest that the introduction of Ni species can obviously affect the mesostructures of the ceria materials. In addition, TEM was used as a complementary technique to examine the structures of the ceria-based samples and representative image for the $Ce_{0.90}Ni_{0.10}O$ sample is shown in Fig. 5. The image does not clearly show the presence of the ordered mesopores, yet reveals a rather foam-like structure resulting from closely aggregated metal oxides nanoparticles [29,31].

The XRD patterns of ceria-based samples are illustrated in Fig. 6. No XRD lines pertaining to NiO phase are detected; the result reveals the formation of solid solutions with typical cubic fluorite phases (JCPDS No. 34-0394) of all the Ni-doped ceria samples. For all the samples, the co-precipitation derived $Ce_{0.90}Ni_{0.10}O$-CP sample demonstrates the strongest diffraction peaks, indicating it has the largest crystallinity and particle size (*ca.* 8.5 nm according in TEM image, not shown here). Moreover, an accurate comparison of the (1 1 1) plane for the ceria-based samples (inset of Fig. 6) suggests that the (1 1 1) diffraction peak of the Ni-doped ceria sample shifts

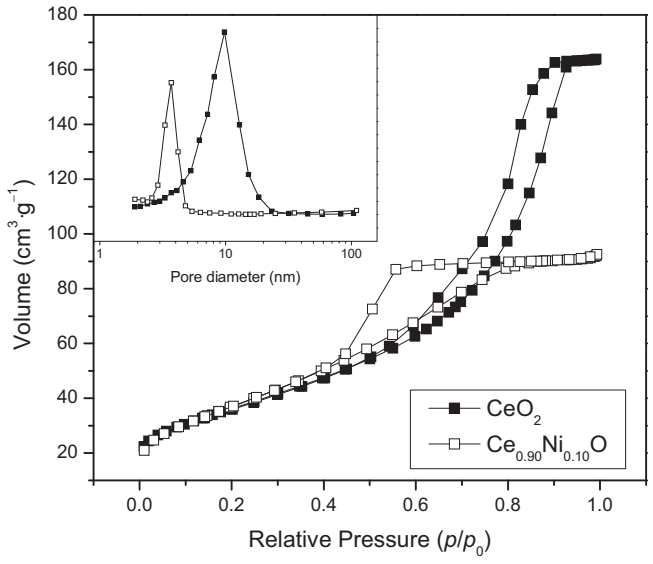

Fig. 4. N_2 adsorption–desorption isotherm and pore size distribution of CeO_2 and $Ce_{0.90}Ni_{0.10}O$ samples.

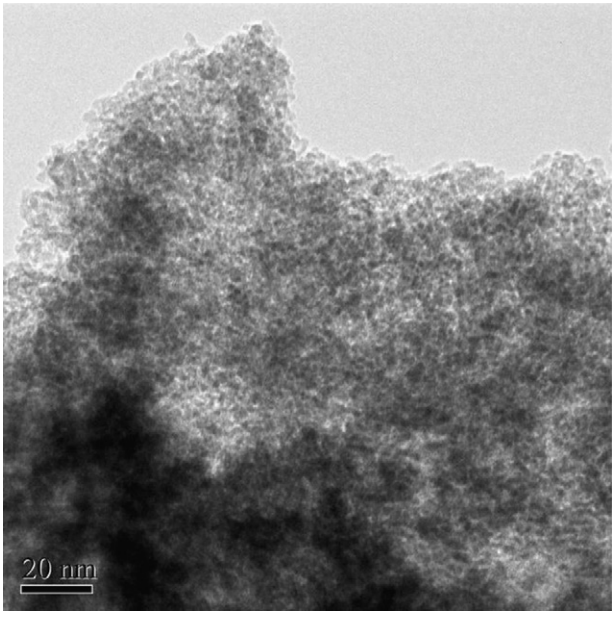

Fig. 5. TEM image of $Ce_{0.90}Ni_{0.10}O$ sample.

Table 3
Textural properties and TPR profiles of CeO_2 and doped ceria materials.

Catalyst	S_{BET} ($m^2\,g^{-1}$)	V_{pore} ($cm^3\,g^{-1}$)	Pore size (nm)	H_2-TPR T_M (°C)[a]	H_2 consumption of Peak α ($mmol\,g^{-1}$)
$Ce_{0.90}Al_{0.10}O$	144	0.19	4.5	506	0.76
$Ce_{0.90}Sn_{0.10}O$	145	0.15	3.5	360	0.84
$Ce_{0.90}Zr_{0.10}O$	126	0.16	4.6	468	0.63
$Ce_{0.90}Mn_{0.10}O$	149	0.33	4.5	304	1.15
$Ce_{0.95}Ni_{0.05}O$	153	0.47	7.6	316	1.45
$Ce_{0.90}Ni_{0.10}O$	134	0.36	3.7	286	1.66
$Ce_{0.80}Ni_{0.20}O$	114	0.24	3.2	287	1.52
$Ce_{0.90}Ni_{0.10}O$-CP	71	0.13	6.4	322	1.22
CeO_2	175	0.54	9.8	508	1.60

[a] Temperature of the maximum H_2 consumption (T_M).

to the higher 2θ angle, compared with the pristine ceria sample. The reason is that the replacement of Ce^{4+} (0.97 Å) [6] with smaller Ni^{2+} ions (0.84 Å) leads to a further shrinkage of ceria lattice. Among all the Ni-doped CeO_2 samples, the $Ce_{0.90}Ni_{0.10}O$ sample demonstrates the highest angle which implied the smallest unit-cell parameter. Generally, it is proposed that the formation of the solid solution of Ce–Ni–O by the incorporation of Ni^{2+} ions into ceria lattice can favor the generation of oxygen vacancies which adsorb oxygen easily [14,32]. As a result, a large amount of highly reactive oxygen species are formed over the doped ceria sample and the species can be easily reduced by H_2 and other hydrocarbons.

The redox behavior of the pure CeO_2 and Ni-doped ceria samples has been investigated by TPR experiment (Fig. 7). Two main reduction peaks have been identified for all the samples: peak α (280–550 °C) and peak β (750–820 °C), generally attributed to the reduction of surface-capping oxygen and bulk oxygen species respectively [33,34]. While the pure ceria exhibits a broad reduction temperature in the range 250–550 °C, the introduction of Ni species drastically decreases the temperature of peak α. Upon increasing the amount of Ni, peak α of the $Ce_{1-x}Ni_xO$ samples shifts to the lower temperature and the lowest temperature along with the largest H_2-consumption is obtained over $Ce_{0.90}Ni_{0.10}O$ sample (Table 3). In the case of the $Ce_{0.90}Ni_{0.10}O$-CP sample, the TPR profile confirms that the mesostructured sample could provide superior reducibility to that by the co-precipitation method. For the sake of detailed comparison, the redox behaviors of other doped ceria catalysts were also compared and the corresponding temperatures of the maximum H_2 consumption (T_M) are summarized in Table 3. The relatively higher T_M together with lower H_2 consumption of peak α for $Ce_{0.90}Al_{0.10}O$ and $Ce_{0.90}Zr_{0.10}O$ imply that the two catalysts possess less reactive lattice oxygen and thus demonstrate poor catalytic activity under the reaction conditions.

Combined XRD patterns and TPR profiles, it is clarified that the incorporation of 10 wt% Ni into ceria leads to the smallest unit-cell parameter, and hence a more reactive oxygen species generating over the ceria samples. To elucidate the origin of the superior ODH activity achieved by using ceria-based catalyst, the total OSC of the catalysts has been investigated under anaerobic atmosphere at 450 °C. It is noteworthy that the consumption and replenishment of the lattice oxygen is dynamic between reduction and oxidation environments for ODH reaction. Nevertheless, the contribution of the total OSC to the catalytic behavior remains valuable to study. As illustrated in Fig. 8, the pure ceria presents a limited OSC of *ca.* 0.16 mmol [O] g^{-1}. However, doping with Ni results in a distinct

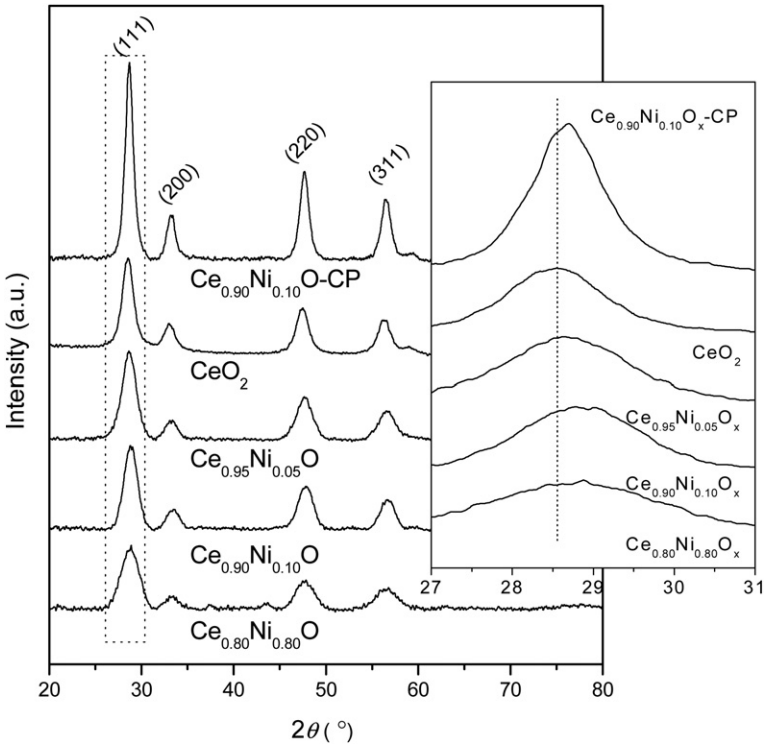

Fig. 6. XRD patterns of CeO_2 and Ni-doped ceria samples.

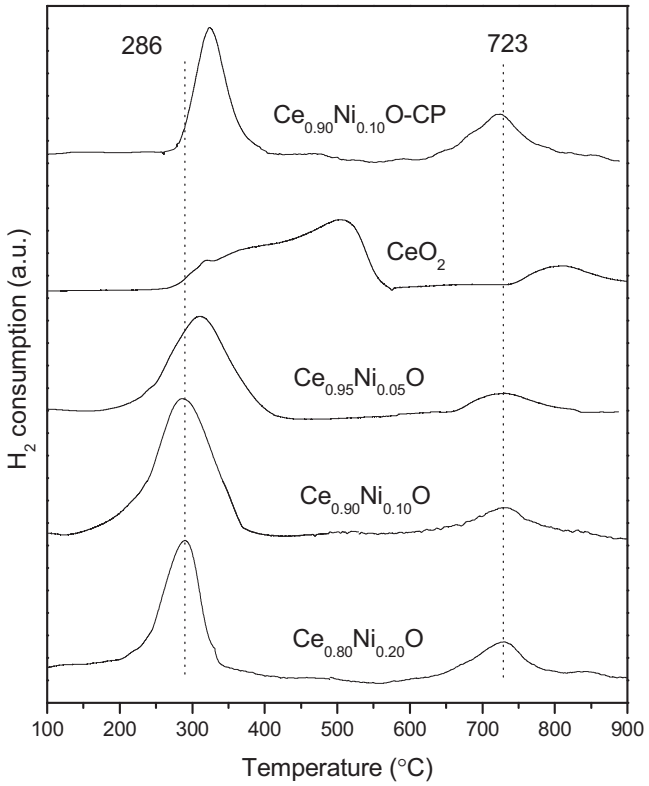

Fig. 7. H_2-TPR profiles of CeO_2 and Ni-doped ceria catalysts.

increase of the total OSC, showing the small amount of Ni would cause a remarkable modification in the oxygen storage behavior of the ceria materials. Significantly, the $Ce_{0.90}Ni_{0.10}O$ sample gives the highest value of OSC (0.52 mmol [O] g^{-1}), compared favorably with other samples. More importantly, the total OSC values over various ceria materials directly correlate the corresponding STY. This points to that the increase of the amount of available surface lattice oxygen species in the ceria contributes directly to their catalytic activity in

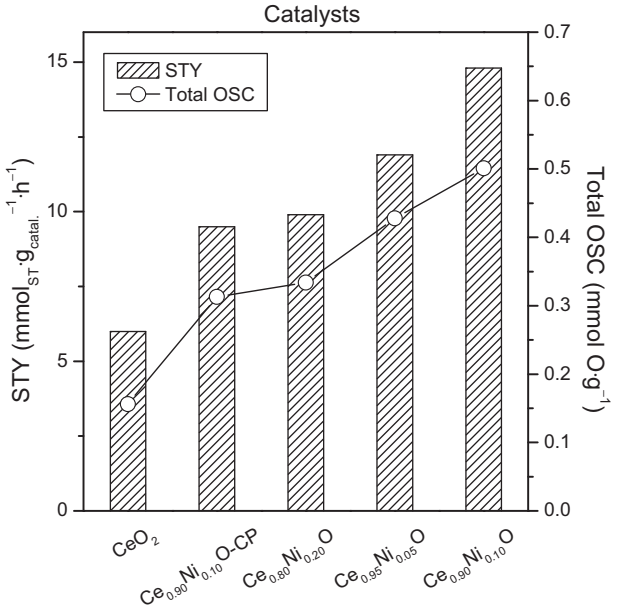

Fig. 8. Correlation between the STY of CeO_2 and Ni-doped ceria catalysts with their corresponding total OSC at 450 °C.

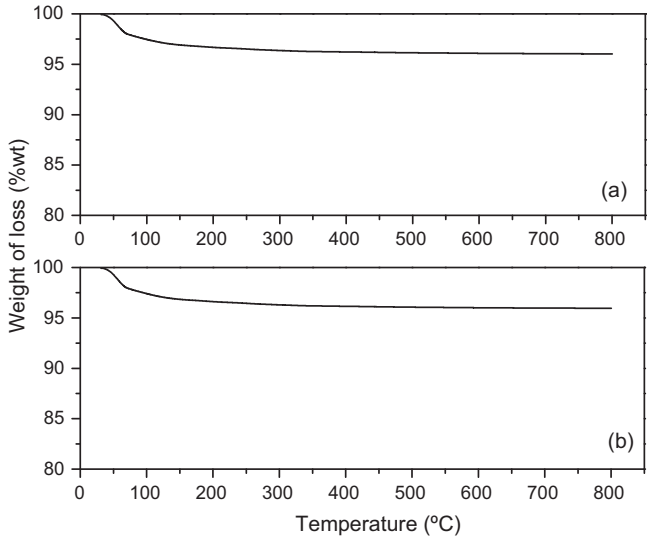

Fig. 9. TG curves of the fresh (a) and spent (b) $Ce_{0.90}Ni_{0.10}O$ samples.

the ODH of EB reaction, permitting a rational explanation for the positive effect of the incorporation of Ni into ceria structure.

With regard to the essential active phase of previously established transition-metal-oxide and phosphate-based catalysts [1,2] for the ODH of ethylbenzene, it is widely believed that the carbon deposits detected on these catalysts are indispensable for the genesis of "true" catalytically active sites for the ODH reaction. Specifically, it has been suggested that the surface redox couples consisting of strongly basic adjacent (quinoidic) oxygen groups of the carbon deposits are responsible for the actual activity observed for these materials [1]. To elucidate the active phase in the present ceria-based catalytic system for the ODH of EB, TPO characterization of the spent $Ce_{0.90}Ni_{0.10}O$ sample (at 12 h TOS) was conducted using flowing air in the TGA mode; the results are compared in Fig. 9. The fact that no carbon deposits could be detected over the used $Ce_{0.90}Ni_{0.10}O$ sample (see Fig. 9b) strongly indicates that the "carbon deposits" mechanism is not applicable for the present ceria-based catalysts in the ODH of EB.

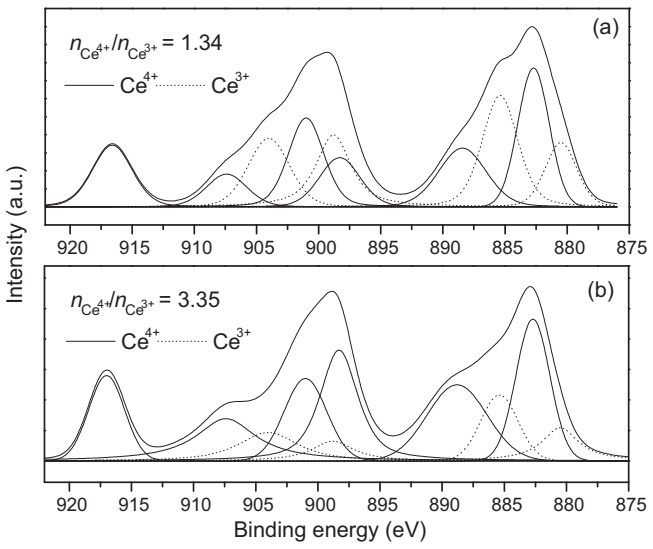

Fig. 10. XP spectra (Ce 3*d*) of an O_2-pretreated $Ce_{0.90}Ni_{0.10}O$ sample after exposure to (a) EB/N_2 and (b) O_2/N_2 stream (10 mL min^{-1}) at 450 °C for 0.5 h. *Note*: The as-analyzed surface fraction of Ce^{3+} species in (a) could be somewhat underestimated as the measurement is not performed *in situ*.

We therefore infer that the present ODH of EB over the doped CeO_2 catalysts may proceed *via* a simple surface redox (Mars-van Krevelen) mechanism [35,36] involving the Ce^{4+}/Ce^{3+} couple, in which the catalyst undergoes reduction (by EB) and reoxidation (by O_2) cycles. In this context, the overall reaction pathway can be envisaged to involve a delicate redox mechanism involving the Ce^{4+}/Ce^{3+} couple during the EB ODH process, i.e. the reaction proceeds by a facile oxygen-transfer mechanism in which the consumption and replenishment of the ceria lattice surface oxygen species play a key role in the reaction process. To testify this hypothesis, XPS studies on $Ce_{0.90}Ni_{0.10}O$ subjected to sequential EB/O_2 exposures were carried out. The results show that the consumption and replenishment of the lattice oxygen, as reflected by the distinct atmospheric-dependent variation of the ratio of Ce^{4+}/Ce^{3+}, is essential for this reaction. These findings constitute a deep insight for the design and development of ceria-based catalyst system that exhibits improved activity for the ODH of EB (Fig. 10).

4. Conclusions

In summary, an efficient mesostructured doped ceria catalyst with high surface area has been developed for the ODH of EB to ST using O_2 as oxidant. Among various metal-doped ceria catalysts investigated, the Ni-doped samples have demonstrated superior catalytic activity for the ODH of EB. N_2 adsorption–desorption results exhibit that template-assisted precipitation method derived Ni-doped samples possess mesostructures with large surface areas. Combined TPR and total OSC results confirm that, in compared with pure ceria sample, Ni-doped ceria samples present easily reducible oxygen species and improved total oxygen storage capacity. Our results show that best catalytic performance can be attainted over the $Ce_{0.90}Ni_{0.10}O$ catalyst which allowing a steady ST yield of 14.8 $mmol_{ST}\ g_{catal.}{}^{-1}\ h^{-1}$ at 450 °C. The high catalytic activity and stability of the Ni-doped catalyst have been contributed to the enhanced oxygen mobility, and modifications of structure by introducing Ni species, respectively. Furthermore, the XPS results imply that the ODH of EB over the doped ceria catalysts may process *via* a simple surface redox mechanism involving Ce^{4+}/Ce^{3+} couple.

Acknowledgments

This work was supported by the the National Natural Science Foundation of China (21076027), Open Foundation of Shanghai Key Laboratory of Molecular Catalysts and Innovative Materials (2011MCIMKF01), the Natural Science Foundation of Jiangsu High School (11KJD150001), and the Project Funded by the Priority Academic Program Development of Jiangsu Higher Education Institutions.

References

[1] F. Cavani, F. Trifiro, Appl. Catal. A 133 (1995) 219–239.
[2] F.M. Bautista, J.M. Campelo, D. Luna, J.M. Marinas, R.A. Quiros, A.A. Romero, Appl. Catal. B 70 (2007) 611–620.
[3] J.A. Maciá-Agulló, D. Cazorla-Amorós, A. Linares-Solano, U. Wild, D.S. Su, R. Schlögl, Catal. Today 102–103 (2005) 248–253.
[4] J. Xu, J. Huang, Y.M. Liu, Y. Cao, Y.X. Li, K.N. Fan, Catal. Lett. 141 (2011) 198–206.
[5] E.H. Lee, Catal. Rev. 8 (1973) 285–305.
[6] B.M. Reddy, P. Lakshmanan, P. Loridant, Y. Yamada, T. Kobayashi, C. Lopez-Cartes, T.C. Rojas, A. Fernandez, J. Phys. Chem. B 110 (2006) 9140–9147.
[7] P. Kuśtrowski, M. Zbroja, R. Dziembaj, H. Papp, Catal. Lett. 80 (2002)1–6.
[8] T.J. Zhao, W.Z. Sun, X.Y. Gu, M. Ronning, D. Chen, Y.C. Dai, W.K. Yuan, A. Holmen, Appl. Catal. A 323 (2007) 135–146.
[9] D.S. Su, N.I. Maksimova, G. Mestl, V.L. Kuznetsov, V. Keller, R. Schlögl, N. Keller, Carbon 45 (2007) 2145–2151.
[10] P. Kustrowski, Y. Segura, L. Chmielarz, J. Surman, R. Dziembaj, P. Cool, E.F. Vansant, Catal. Today 114 (2006) 307–313.
[11] D.B. Tagiyev, G.O. Gasimov, M.I. Rustamov, Catal. Today 102–103 (2005) 197–202.
[12] R. Craciun, N. Dulamita, Ind. Eng. Chem. Res. 38 (1999) 1357–1363.
[13] W. Oganowski, J. Hanuza, L. Kepiski, Appl. Catal. A 171 (1998) 145–154.
[14] B.M. Reddy, K.N. Rao, G.K. Reddy, A. Khan, S.E. Park, J. Phys. Chem. C 111 (2007) 18751–18758.
[15] N. Keller, N.I. Maksimova, V.V. Roddatis, M. Schur, G. Mestl, Y.V. Butenko, V.L. Kuznetsov, R. Schlögl, Angew. Chem. Int. Ed. Engl. 41 (2002) 1885–1888.
[16] J.J. Delgado, D.S. Su, G. Rebmann, N. Keller, A. Gajovic, R. Schlögl, J. Catal. 244 (2006) 126–129.
[17] P. Li, T. Li, J.H. Zhou, Z.J. Sui, Y.C. Dai, W.K. Yuan, D. Chen, Microporous Mesoporous Mater. 95 (2006) 1–7.
[18] A. Rinaldi, J. Zhang, J. Mizera, F. Girgsdies, N. Wang, S.B.A. Hamid, R. Schlögl, D.S. Su, Chem. Commun. (2008) 6528–6530.
[19] S. Bernal, G. Blanco, M.A. Cauqui, M.P. Corchado, C. Larese, J.M. Pintado, J.M. Rodriguez-Izquierdo, Catal. Today 53 (1999) 607–612.
[20] A. Trovarelli, G. Dolcetti, C. Deleitenburg, J. Kaspar, P. Finetti, A. Santoni, J. Chem. Soc., Faraday Trans. 88 (1992) 1311–1319.
[21] R.S. Monteiro, L.C. Dieguez, M. Schmal, Catal. Today 65 (2001) 77–89.
[22] D. Andreeva, V. Idakiev, T. Tabakova, L. Ilieva, P. Falaras, A. Bourlinos, A. Travlos, Catal. Today 72 (2002) 51–57.
[23] D. Andreeva, I. Ivanov, L. Ilieva, M.V. Abrashev, Appl. Catal. A 302 (2006) 127–132.
[24] L.W. Jia, M.Q. Shen, J.J. Hao, T. Rao, J. Wang, J. Alloys Compd. 454 (2008) 321–326.
[25] M.Q. Shen, J.Q. Wang, J.C. Shang, Y. An, J. Wang, W.L. Wang, J. Phys. Chem. C 113 (2009) 1543–1551.
[26] B.M. Reddy, A. Khan, Y. Yamada, T. Kobayashi, S. Loridant, J.C. Volta, J. Phys. Chem. B 107 (2003) 5162–5167.
[27] J. Xu, L.C. Wang, Y.M. Liu, Y. Cao, H.Y. He, K.N. Fan, Catal. Lett. 133 (2009) 307–313.
[28] M.F. Luo, J.M. Ma, J.Q. Lu, Y.P. Song, Y.J. Wang, J. Catal. 246 (2007) 52–59.
[29] D. Terribile, A. Trovarelli, J. Llorca, C. de Leitenburg, G. Dolcetti, J. Catal. 178 (1998) 299–308.
[30] Q. Liu, L.-C. Wang, M. Chen, Y. Cao, H.-Y. He, K.-N. Fan, J. Catal. 263 (2009) 104–113.
[31] Y.J. Wang, J.M. Ma, M.F. Luo, P. Fang, M. He, J. Rare Earth 25 (2007) 58–62.
[32] L. Ilieva, G. Pantaleo, R. Nedyalkova, J.W. Sobczak, W. Lisowski, M. Kantcheva, A.M. Venezia, D. Andreeva, Appl. Catal. B 90 (2009) 286–294.
[33] S. Scire, S. Minico, C. Crisafulli, C. Satriano, A. Pistone, Appl. Catal. B 40 (2003) 43–49.
[34] A.M. Venezia, G. Pantaleo, A. Longo, G. Di Carlo, M.P. Casaletto, F.L. Liotta, G. Deganello, J. Phys. Chem. B 109 (2005) 2821–2827.
[35] K. Chen, A. Khodakov, J. Yang, A.T. Bell, E. Iglesia, J. Catal. 186 (1999) 325–333.
[36] K. Chen, E. Iglesia, A.T. Bell, J. Catal. 192 (2000) 197–203.
[37] J. Zhang, D.S. Su, A.H. Zhang, D. Wang, R. Schlögl, C. Hebert, Angew. Chem. Int. Ed. Engl. 46 (2007) 7319–7323.